RSC Advances

PAPER

Cite this: *RSC Adv.*, 2023, **13**, 21318

Highly selective optical sensor N/S-doped carbon quantum dots (CQDs) for the assessment of human chorionic gonadotropin β-hCG in the serum of breast and prostate cancer patients

Yasmeen M. AlZahrani,[a] Salha Alharthi,[a] Hind A. AlGhamdi,[a] A. O. Youssef,[b] Shahenda S. Ahmed,[b] Ekram H. Mohamed,[c] Safwat A. Mahmoud*[d] and Mohamed S. Attia*[b]

A low-cost, accurate, and highly selective method was used for the assessment of the human chorionic gonadotropin β-hCG in the serum of breast and prostate cancer patients. This method is based on enhancing the intensity of luminescence displayed by the optical sensor N/S-doped carbon dots (CQDs) upon adding different concentrations of β-hCG. The luminescent optical sensor was synthesized and characterized through absorption and emission and is tailored to present blue luminescence at λ_{em} = 345 nm and λ_{ex} = 288 nm at pH 7.8 in DMSO. The enhancement of the luminescence intensity of the N/S-doped CQDs, especially, the characteristic band at λ_{em} = 345 nm, is typically used for determining β-hCG in different serum samples. The dynamic range is 1.35–22.95 mU mL^{-1}, and the limit of detection (LOD) and quantitation limit of detection (LOQ) are 0.235 and 0.670 mU mL^{-1}, respectively. This method was practical, simple, and relatively free from interference effect. It was successfully applied to measure PCT in the samples of human serum, and from this method, we can assess some biomarkers of cancer-related diseases in human body.

Received 9th March 2023
Accepted 4th July 2023

DOI: 10.1039/d3ra01570j

rsc.li/rsc-advances

1. Introduction

The discovery of carbon dots (CDs) was mainly in 2004 during the sorted single-walled carbon nanotube (SWCNT) purification process *via* preparative electrophoresis. CDs are classed as a novel fluorescent small carbon nanomaterial with less than 10 nm particle size.[1–3]

Carbon dots (CDs) are highly-emissive nanoparticles obtained through fast and cheap syntheses as a new type of carbon-based nanomaterial. They have attracted considerable attention of researchers for years owing to their diverse physicochemical properties and promising attributes, such as high biocompatibility and unique optical properties. These nanomaterials have outstanding water solubility with low toxicity and low production cost and offer tunable fluorescence emission and excitation. They are photochemically and physicochemically stable, eco-friendly, and have abundant functional groups (*e.g.*, amino, hydroxyl, and, carboxyl), high stability, superficial synthesis methods, easy surface modification, and electron mobility.[2–4]

Carbon dots (CDs) have a wide range of applications in bio-imaging fields, bio-sensing, drug-gene delivery system, disease discovery, synthetic chemistry, *in vitro* and *in vivo* bio-imaging, chemical and biological sensing, and photodynamic and photothermal therapies. The development of various morphologies, sizes, and target-specific carbon dots represent future areas of study.[3]

Human chorionic gonadotropin (HCG) is a glycoproteinhormone endogenously secreted by the placenta that is composed of 2 noncovalently linked molecules, namely, the α and the β subunits. The earliest indication of an association between HCG and neoplasms was the identification of HCG as a tumor marker.[5]

The β-subunit of the peptide hormone (β-hCG) was recognized in different germ cell and non-germ cell tumors, and it was used previously to monitor response to treatment and to detect tumor relapse.[6] The elevated level of β-hCG was observed in prostate[7] and breast cancer[8] patients. The diagnosis of breast cancer in the current scenario is done by mammogram, MRI and, MR spectroscopy, and breast biopsy tests. All these detection techniques are very costly and time-consuming, involve surgical techniques, and the results are sometimes negative. Hence, there is a need to develop a cost-effective technique that

[a]*Chemistry Department, College of Science, Imam Abdulrahman Bin Faisal University, P.O. Box 1982, 31441, Dammam, Saudi Arabia*
[b]*Chemistry Department, Faculty of Science, Ain Shams University, Abbassia, Cairo, 11566, Egypt. E-mail: Mohamed_sam@yahoo.com*
[c]*Analytical Chemistry Department, The British University in Egypt, El Sherouk City, Cairo, 11378, Egypt*
[d]*Physics Department, Faculty of Science, Northern Border University, Arar, Saudi Arabia*

can qualitatively and/or quantitatively detect breast cancer at an early stage. Therefore, the development of a highly sensitive sensor system for the monitoring of early-stage breast cancer is required, so that the patient can stay alert about the risk of diagnosis.[9]

Several techniques were used to evaluate β-hCG, such as immunologic and reverse transcriptase-polymerase chain reaction (RT-PCR), in prostate cancer,[10] but different studies[11] showed that they did not help. It was reported that hCG is not detected in normal prostate tissues, but is specific for low-grade prostate cancer,[10] resulting in a lack of quantification in these studies.

In this study a highly selective and straightforward analytical strategy was adopted for the accurate, fast, and affordable determination of human chorionic gonadotropin β-hCG in the serum of breast and prostate cancer patients. It depends on enhancing the luminescence intensity of N/S-doped carbon dot optical sensor after the addition of β-hCG with different concentrations. The newly designed sensor was fabricated and characterized *via* absorption and emission specifications and is customized to exhibit blue luminescence in DMSO at a λ_{em} of 345 nm when excited at 288 nm. The main mechanism through which the sensor functions is the fluorescence resonance energy transfer (FRET). The obtained results were statistically analyzed and were found to be satisfactory. The limit of detection of the suggested probe was 6.7×10^{-10} mIU mL^{-1} with a correlation coefficient of 0.98.

2. Experimental

2.1. Instrumentation

A double-beam UV-Vis spectrophotometer (model: Edinburgh Instruments DS5) equipped with a Xenon flash lamp with a spectral range of 190–1100 nm. A spectrofluorometer (Edinburgh Instruments FS5) having a spectral range up to 1650 nm and fluorescence lifetimes down to 25 ps. A pH meter (model: Jenway-3040). A Daihan Scientific centrifuge device (model: CF-10). Fourier transform infrared (FTIR) (model: Shimadzu-FTIR-8400 S, Japan). The structures of the phases formed were examined using a high-resolution transmission electron microscope (HR-TEM) with an acceleration voltage up to 200 kV (JEM-2100-JEOL, Japan). The oxidation states and species in the prepared materials were determined by a Thermo Scientific™ K-Alpha™ X-ray photoelectron spectrometer (XPS) (Thermo Scientific, USA), using Al-K_α microfocused monochromator within an energy range up to 4 keV. The X-ray diffraction (XRD) analysis of N/S-doped QDs was performed with a D8-AVANCE X-ray diffractometer (Bruker, Germany) with Cu-Kα radiation (λ = 0.154056 nm) for the identification of the crystalline phase, relative crystallinity, and crystal size of the as-prepared N/S-doped QDs. The XRD analysis was performed in the 2θ range from 3.0° to 80.0° with a 0.020° step at a scan speed of 0.4 s.

2.2. Materials

Ethanol, acetonitrile, dimethyl sulfoxide (DMSO), and dimethyl formamide (DMF), citric acid monohydrate, and thiourea (TU) were purchased from Sigma-Aldrich. Human chorionic gonadotropin (β-hCG) was purchased from BioMérieux, Inc. Human serum samples were collected from Raba'a El-Adwyea hospital (Nasr city, Egypt). The procedure for collecting human specimens was carried out in compliance with World Health Organization (WHO) approval. The ethics committee at Ain Shams University gave its approval for all tests to be carried out in accordance with the guidelines established by the "Ministry of Health and Population, Egypt." The humans participating in this study provided informed consents.

2.3. Reagents and solutions

2.3.1. Preparation of N/S-doped CQDs. The N/S-doped CQDs was prepared by the carbonization of citric acid in a similar method reported previously with some modification.[12] Briefly, 1.0 g of citric acid and 0.5 g of thiourea (TU) were ground and mixed thoroughly to make it homogenous. The solid mixture was transferred to a 100 mL beaker and heated to 200 °C in a muffle for 20 min. A brownish-yellow thick syrup solution was obtained from the thermal process. After cooling to room temperature, the thick solution was diluted to 100 mL with Milli-Q water and then subjected to dialysis in a dialysis bag (M.W. cutoff: 5 kDa). Fig. 1.

2.3.2. Stock and working solutions. The concentration of the stock solution of N/S-doped CQDs is 1×10^{-2} mol L^{-1}. The Stock solution of β-hCG was prepared by dissolving 0.5 g of N/S-doped CQDs in 2 mL deionized distilled water. In a 25 mL volumetric flask, the working solution of N/S-doped CQDs was obtained by transferring 0.25 mL of the stock solution of N/S-doped CQDs into DMSO solvent, and the volume was adjusted to the mark to obtain a final concentration of 1×10^{-4} mol L^{-1}. To prepare β-hCG working solution, 400 μL from its corresponding stock solution was accurately added to 2 mL water. From the later working solution, a calibration set for β-hCG was

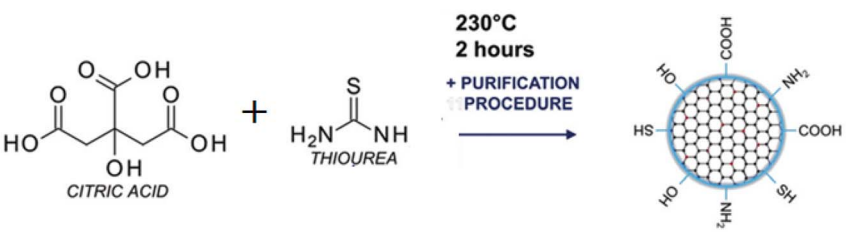

Fig. 1 Scheme for the preparation of N/S-doped CQDs.

prepared. When not in use, all stock and working solutions were kept at 2–8 °C. The stated procedures were followed for performing the subsequent measurements of absorption and emission spectra and pH, molar ratio, and solvent effects. The intensity of luminescence was recorded at $\lambda_{ex}/\lambda_{em} = 288/345$ nm.

2.4. General procedure

2.4.1. Calibration curve. The optical probe N/S-doped CQDs was thoroughly mixed with the standard solution of β-hCG with different concentrations, as previously detailed, in the spectrophotometer cell. The luminescence spectra were then recorded at the chosen $\lambda_{ex} = 288$ nm. Then, a relation between the peak intensity on *Y*-axis against the concentration of β-hCG on *X*-axis was drawn.

2.4.2. Determination of β-hCG in serum samples. 1.0 mL of blood sample each from 11 healthy volunteers were collected and centrifuged for 15 min at 4000 rpm to remove proteins. The concentration of β-hCG was determined from the corresponding calibration graph.

3. Results and discussion

3.1. FT-IR spectrum

Fourier transform infrared (FT-IR) spectroscopy was applied to confirm the surface functional groups of the N/S-doped CQD sensor. As shown in Fig. 2A, FT-IR spectra exhibit the peaks of O–H bending and stretching vibrations at 671 and 3679 cm^{-1}, respectively. The peak at 3444 cm^{-1} in 3000–3744 cm^{-1} range represents N–H stretching vibrations.[13–15] The peak at 1253 cm^{-1} was attributed to O–H in-plane bending vibrations.[16] These considerable amino, hydroxyl hydrophilic groups could enable N,S-CQDs superior hydrophilicity.[17] The peak at 1706 cm^{-1} is attributed to the stretch vibration of C=O carboxylic groups and C=N bonds,[18] and the two peaks at 1646 and 1516 cm^{-1} are characteristic to the vibration of amide group stretching C=O (amide I) and the in-plane bending of N–H bond (amide II),[18,19] respectively. The peak at 1072 cm^{-1} is attributed to C–O stretching vibrations.[20] Then, the peaks at 1595 and 1695/1741 cm^{-1} are attributed to C=C and C=O stretching vibrations, respectively.[21,22] The peaks at 1427 and 1395 cm^{-1} can be assigned to the vibrations of C–S and C–N, respectively,[23] and the peak at 1184 cm^{-1} further confirm the existence of C–O bond.[17,23]

3.2. TEM, XRD and XPS measurements

To reveal the size and morphology of the N/S-doped CQDs, HRTEM was employed, and the result is presented in Fig. 2B. HR-TEM images showed spherical N/S-doped CQDs with a narrow size distribution (1.6–3.7 nm) and an average size of 2.8 nm. The XRD pattern (Fig. 2C) displayed a broad peak ($2\theta \approx 26.100°$), which corresponded to the (002) plane. The result is similar to that of graphite and indicated the presence of highly disordered carbon atoms.[24–26] Although XRD measurement is the best technique to evaluate the structure of N/S-doped CQDs, results from FT-IR spectroscopy, XPS, and UV-Vis measurements are also very helpful. In general,

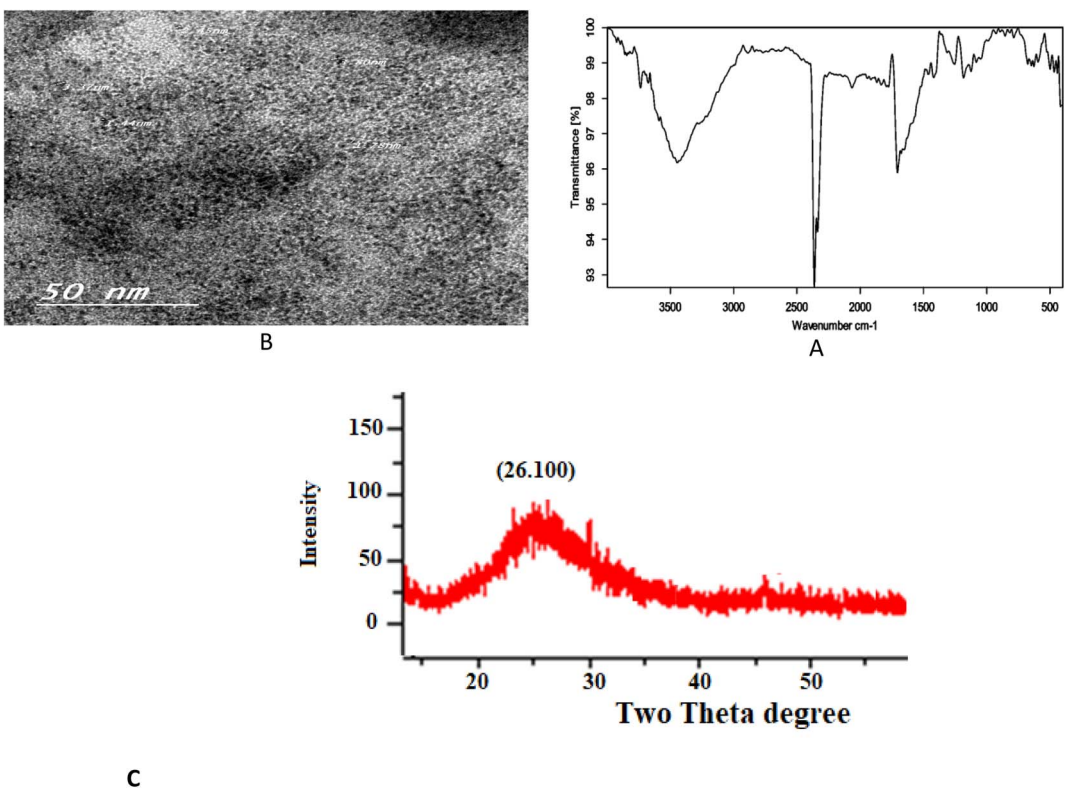

Fig. 2 (A) TEM image, (B) FT-IR spectrum, and (C) XRD patterns.

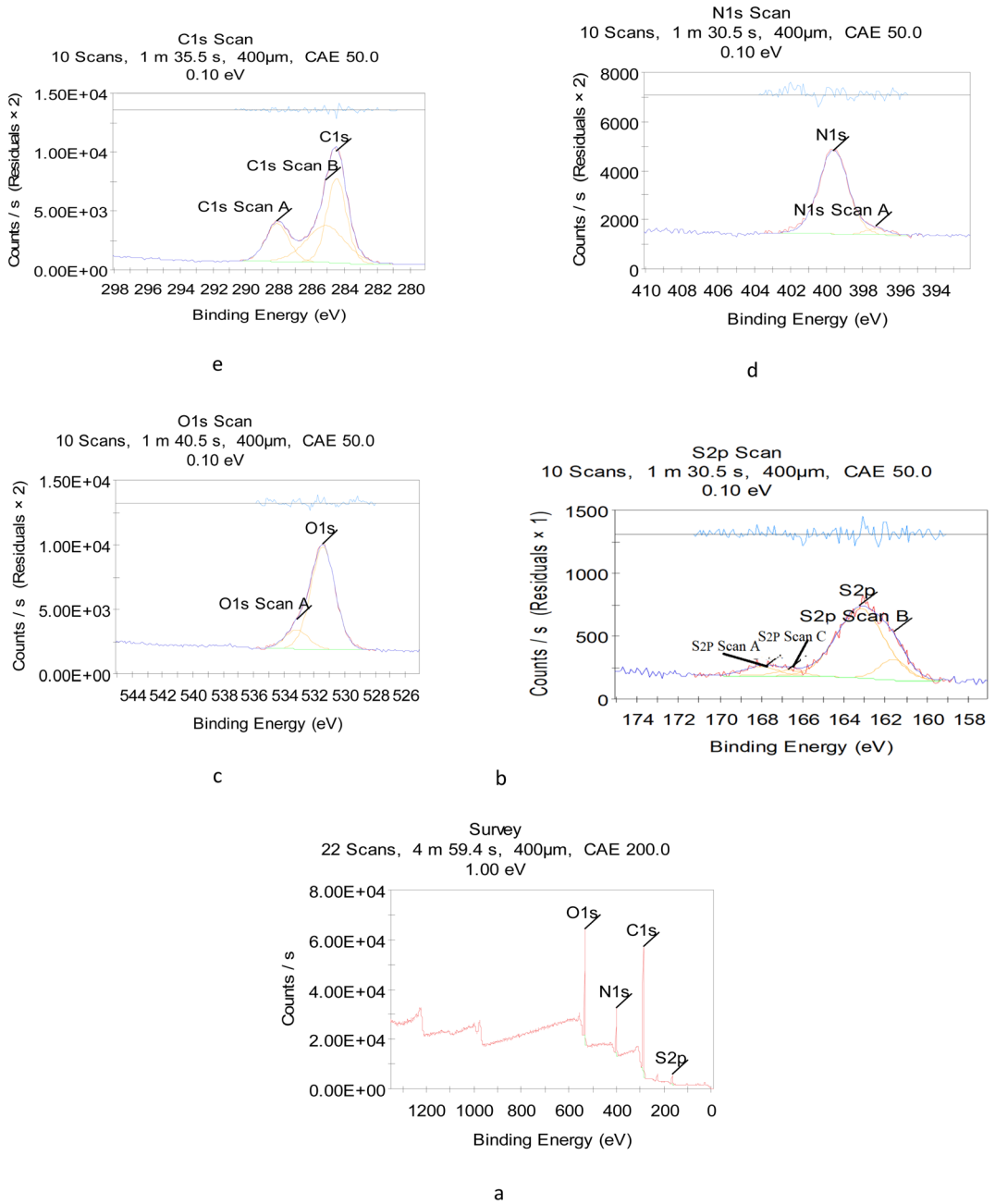

Fig. 3 XPS (a) full survey, (b) S 2p, (c) O 1s, (d) N 1s, and (e) C 1s spectra.

amorphous N/S-doped CQDs are mainly composed of sp^3 carbons, whereas crystalline CDs have sp^2 hybridized carbon domains.[27,28] As will be discussed in the next few sections, the results from XPS, FT-IR spectroscopy, and UV-Vis measurements showed the presence of sp^3 and sp^2 carbon structures. Hence, these results could demonstrate the coexistence of crystalline and disordered (amorphous) carbon domains in the N/S-doped CQD structure. In addition, from the XPS survey spectrum (Fig. 3a), the peaks at 531.08, 398.08, 284.08, and 162.08 eV could be related to O 1s, N 1s, C 1s, and S 2p, respectively.[29] The two peaks presented in the high-resolution XPS of S2P (Fig. 3b) at 162.38 and 166.78 eV could be assigned to $2p_{3/2}$ (–C–S–C– covalent bond) and S–O bonding, respectively.[30,31] Also, high-resolution XPS of O 1s (Fig. 3c) showed the presence of covalent O and ketonic O atoms (peaks at 534 and 530 eV).[32] N 1s (Fig. 3d) showed the presence of pyridinic N atoms (peak at 398.50 eV).[32] However, the deconvoluted peak of C 1s showed the presence of three peaks, which can be attributed to the sp^2 C in graphene (283.68 eV), sp^3 C from C–N/C–S and C–O (285.25 eV), and carboxyl groups (288.4 eV) (Fig. 2E).[33] More interestingly, XPS and FT-IR spectroscopy results are in agreement with each other and proved the presence of various surface functional groups and effective doping of S and N atoms into CQDs.

3.3. Absorption spectra

Depending on the solvent's polarity, the aprotic solvent used in UV-Vis absorption and the emission fluorescence spectra of the C-dots influenced the positions and intensity. The absorption spectra of the N/S-doped CQD sensor in different solvents are shown in Fig. 4, indicating a high absorption in DMSO solvent.

The absorption spectra of N/S-doped CQD sensor in DMSO with different concentrations of β-hCG are illustrated in Fig. 5. Spectrum[1] represents the absorption spectrum of free N/S-doped CQDs exhibiting a prominent peak at 260 nm and a tail extending into the visible range. This is attributed to the n–π* transition of C=O bond and π–π* transition of C=C bond electronic transitions in N/S-doped CQD rings.[14,34,35] While spectra 2, 3, and 4 indicate higher absorption after the addition of 5.4, 45.9, and 72.9 mU mL^{-1} of β-hCG, respectively.

3.4. Emission spectra

The emission spectra of N/S-doped CQDs in different concentrations of β-hCG show that the intensity of the characteristic peak at λ_{em} = 345 nm of N/S-doped CQDs is enhanced due to energy transfer from the optical sensor to β-hCG, Fig. 6. The mechanism of the energy transfer is taken place by electron transfer from the *N*-linked protein glycosylation (*N*-glycosylation of *N*-glycans) at Asn residues (Asn-*x*-Ser/Thr motifs) in the glycoproteins of β-hCG to the N/S-doped CQDs. The *N*-linked protein glycosylation is a post-translational modification that occurs in many glycoproteins, including β-hCG. In this modification, a sugar molecule is attached to the Asn residue of the protein. The sugar molecule has a negative charge, which attracts the positively charged N/S-doped CQDs. This attraction brings the N/S-doped CQDs close to the protein, and allows for the electron transfer to occur. The electron transfer from the protein to the N/S-doped CQDs causes an increase in the energy of the CQDs. This increase in the energy is released as light, which enhanced the intensity of the characteristic peak at λ_{em} = 345 nm of the N/S-doped CQDs. The energy transfer from the N/S-doped CQDs to β-hCG can be used to detect β-hCG in a sample. The intensity of the characteristic peak at λ_{em} = 345 nm of the N/S-doped CQDs is directly proportional to the concentration of β-hCG in the sample. This means that the intensity of the peak can be used to quantify the concentration of β-hCG in the sample, Fig. 7.

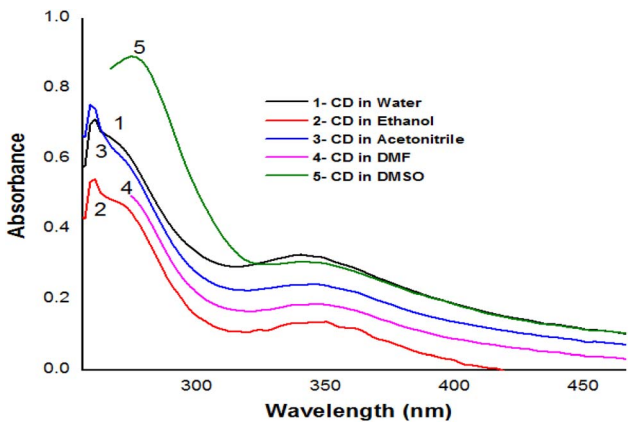

Fig. 4 Absorption spectra of CD sensor in different solvents.

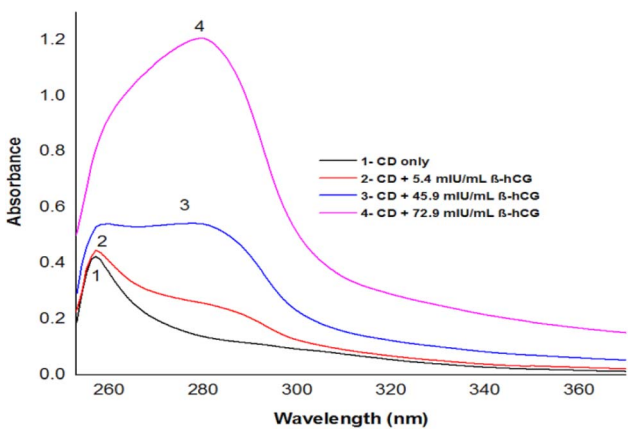

Fig. 5 Absorption spectra of CD sensor in DMSO with different concentrations of β-hCG.

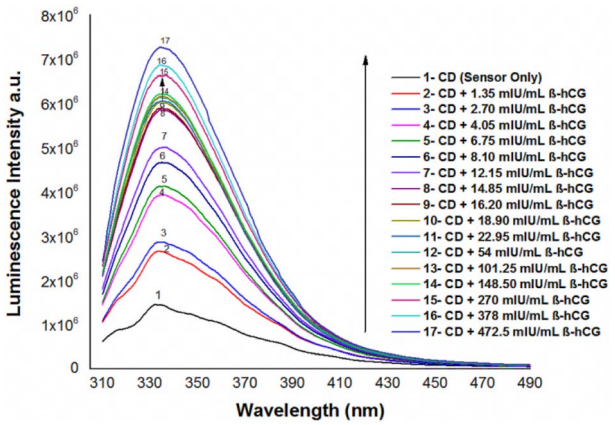

Fig. 6 Luminescence emission spectra of N/S-doped CQDs in the presence of different concentrations of β-hCG in DMSO at λ_{ex} = 288 nm.

3.5. Effect of experimental variables

3.5.1. Effect of solvent. The influence of the solvent on the luminescence intensities of the solutions containing N/S-doped CQDs was studied under the above-mentioned conditions. The results show the enhanced emission of N/S-doped CQDs in DMSO with pH = 7.8, as shown in Fig. 8. Also, the luminescence intensity for the N/S-doped CQDs in the DMSO solution is stronger than in DMF, acetonitrile, water, and ethanol. This can be attributed to the interactions between the solvent and N/S-doped CQDs, which affects the energy difference between the ground and the excited states, and the orientation polarizability of solvents. The dipole moment represents the electron distribution in a molecule with a specific structure. In combination with the reactive field around it, the dipole moment plays an essential role in the transition of a molecule because a molecule can absorb light when its dipole moment changes.[35]

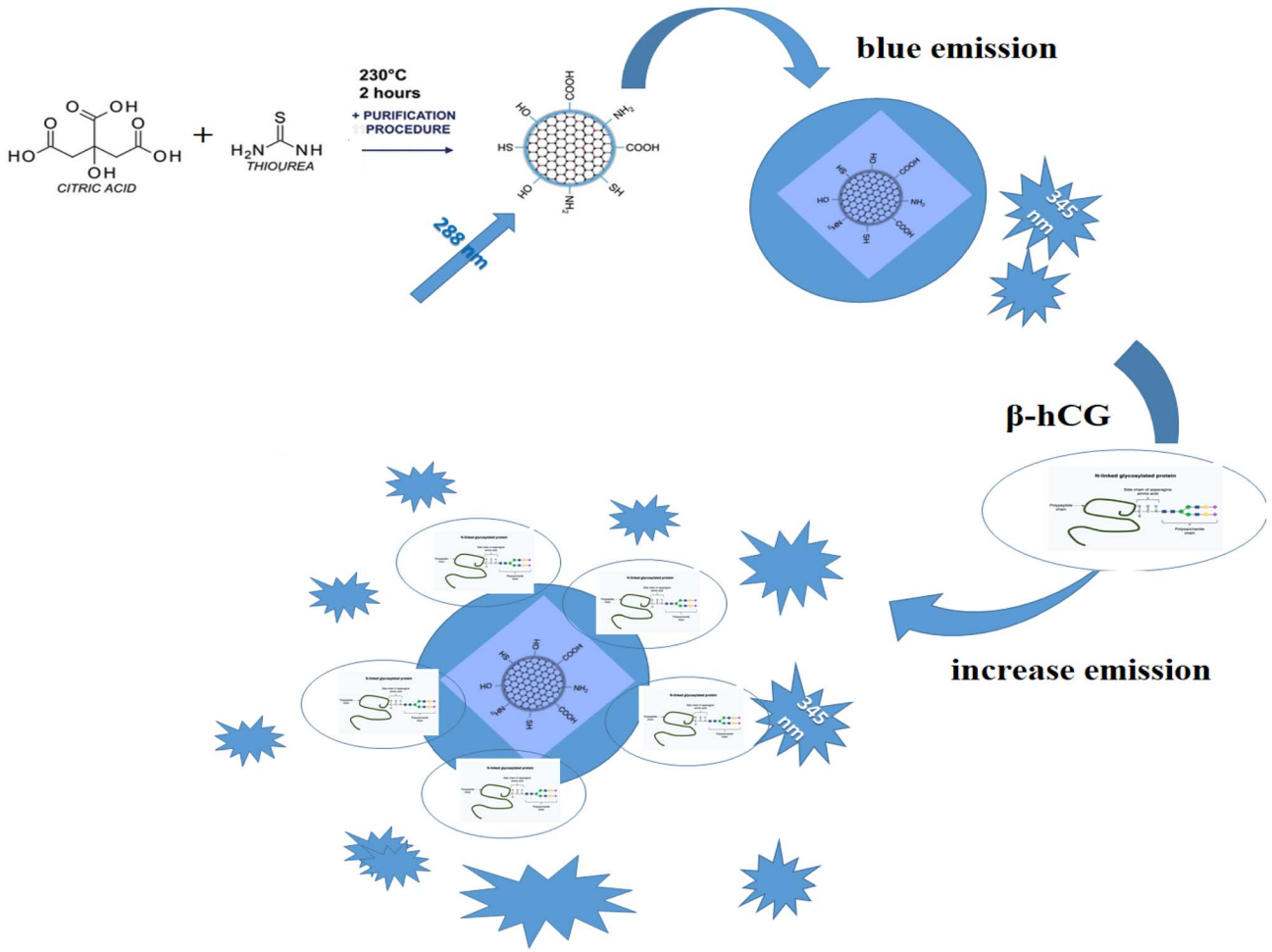

Fig. 7 Mechanism of the energy transfer between β-hCG to the N/S-doped CQD.

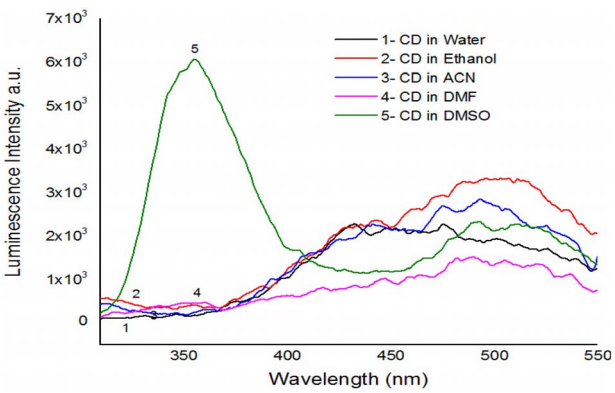

Fig. 8 Luminescence emission spectra of N/S-doped CQDs in the presence of different solvents at $\lambda_{ex} = 288$ nm.

4. Analytical performance

4.1. Method validation

4.1.1. Analytical parameters of optical sensor method. A linear correlation was found between the luminescence intensity of the optical sensor at $\lambda_{em} = 345$ nm and the concentration of β-hCG in the range of 1.35–22.95 mIU mL^{-1}, as shown in Fig. 9, and a calibration curve was obtained by plotting the peak intensity of the N/S-doped CQDs *versus* the concentration of β-hCG at $\lambda_{em} = 345$ nm. The limit of detection (LOD) and quantitation (LOQ) calculated according to the ICH guidelines[36] using the formula: LOD = $3.3S/b$ (equals to 0.234 mIU mL^{-1}) and LOQ = $10S/b$ (equals to 0.67 mIU mL^{-1}) (where S is the

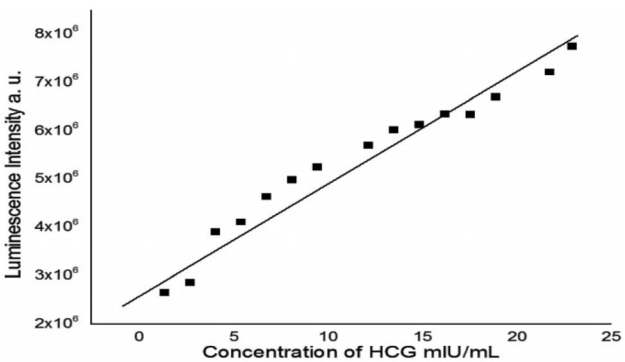

Fig. 9 Linear relationship between the luminescence intensity of N/S-doped CQDs and different concentrations of β-hCG at $\lambda_{em} = 345$ nm.

Table 1 Sensitivity and regression parameters for photo probe[a]

Parameter	Value
λ_{em} (nm)	345
Liner range, (mIU mL^{-1})	1.35–22.95
Limit of detection (LOD), (mIU mL^{-1})	0.670
Limit of quantitation (LOQ) (mIU mL^{-1})	0.236
Regression equation, Y*	$Y = a + bX$
Intercept (a)	2.27×10^{6}
Slope (b)	3.37×10^{5}
Standard deviation	6.86×10^{-5}
Variance (Sa^2)	4.70×10^{-9}
Regression coefficient (r)	0.98

[a] Where Y = fluorescence intensity, X = β-hCG concentration in mIU mL^{-1}, a = intercept, b = slope.

standard deviation of blank luminescence intensity value, and b is the slope of the calibration plot) are also given in Table 1.[37–58]

4.1.2. Selectivity. The method selectivity and validity was investigated by studying the effect of possible interfering substances on the luminescence spectra of the N/S-doped CQDs after the addition of 24 mIU mL^{-1}. The interfering substances included bilirubin (40 mg dL^{-1}), hemoglobin (1 mg dL^{-1}), ascorbic acid (20 mg dL^{-1}), glucose (2000 mg dL^{-1}), and triglycerides (1200 mg dL^{-1}). It was shown that all interfering substances have no significant influence on the luminescence intensity of the N/S-doped CQD sensor.

4.1.3. Application to formulations. For testing the applicability of the proposed method, it was applied for the determination of β-hCG concentration for 11 serum samples of the health state human. The results in Table 2 show that the method is successful for the determination of β-hCG in serum samples. It is clear that the average value of the β-hCG concentration for patients obtained by the proposed method is 30 003 ± 3.91 mIU mL^{-1} and that obtained by the standard method is 30 000 mIU mL^{-1}, highlighting excellent accuracy and precision. The average recovery and RSD for the serum samples in our method found to be 100.35 ± 1.96% and were also presented for comparison and show a good correlation with those of the reference method and with the label claimed.

4.1.4. Recovery study. To further evaluate the accuracy of the method recovery experiments was assessed by determining the agreement between the measured standard concentration and the added known concentration to the sample. In all cases, the values of the recovery percentage ranged between 98.95 and 101.76% with a relative standard deviation in the range of 0.0047–3.92% for serum samples. The closeness of the results to 100% showed the fairly good accuracy of the method.

4.1.5. Accuracy and precision study. For precision computation, the assays were performed in triplicates within the same day and on three different days to determine the repeatability of the method and intermediate precision, respectively. The average percentage relative standard deviation (% RSD) values were calculated and found to be ≤0.0047–1.57% and ≤0.0047–3.92% for intra-day and inter-day precisions, respectively, for the serum samples, indicating the high precision of the proposed method. The inter-day values indicate high precision of the method. Accuracy was assessed as percentage relative error (%RE) between the measured mean concentrations and the known β-hCG concentrations and was determined at each concentration. % RE results are summarized in Table 2 having values ≤0.009–1.76% for intra-day and ≤0.007–1% for inter-day for the serum samples, demonstrating the high accuracy of the proposed method.

Table 2 Evaluation of intra-day an inter-day accuracy and precision[a]

		Propose method									
		Intra-day accuracy and precision (n = 3)					Inter-day accuracy and precision (n = 3)				
		Average found					Average found				
Sample	Standard method average mIU mL^{-1}	mIU mL^{-1}	±CL	% RE	Average recovery	% RSD	mIU mL^{-1}	±CL	% RE	Average recovery	% RSD
Patient (1)	30 000	30 003	±3.91	0.010	100.01	0.005	29 998	±3.92	0.007	99.99	0.005
Patient (2)	21 000	21 002	±2.48	0.009	100	0.0047	21 001	±2.48	0.03	100	0.0047
Patient (3)	920	921.3	±1.29	0.14	100.14	0.056	920.67	±1.88	0.29	100.07	0.08
Patient (4)	863	862.66	±1.41	0.039	99.96	0.066	862	±1.86	0.12	99.88	0.087
Patient (5)	370	370.66	±1.41	0.178	100.18	0.15	370.33	±1.88	0.089	100.09	0.016
Patient (6)	226	225.67	±1.88	0.55	99.85	0.33	226.17	±1.41	0.075	100.07	0.25
Patient (7)	179	178	±2.13	0.56	99.44	0.48	179.77	±0.62	0.43	100.43	0.13
Patient (8)	100	99.90	±0.71	0.10	99.90	0.29	99.98	±0.868	0.02	99.68	0.35
Patient (9)	80	79.16	±1.06	0.625	98.95	0.96	80.63	±1	0.78	100.79	0.54
Patient (10)	48	48.33	±1.88	0.68	100.69	1.57	47.82	±2.20	0.375	99.63	1.80
Patient (11)	17	17.30	±0.63	1.76	101.76	1.44	16.83	±1.6	1	99	3.92

[a] % RE, percent relative error. % RE = [(concentration proposed − concentration known)/concentration known] × 100, % RSD, relative standard deviation. % RSD = [S/(average measurements)] × 100, and ±CL, confidence limits: CL = $tS/n^{(1/2)}$. (The tabulated value of t is 4.303, at the 95% confidence level; S = standard deviation and n = number of measurements).

5. Conclusion

The N/S-doped CQDs exhibited characteristic peaks, which are significantly enhanced in the presence of β-hCG at $\lambda_{ex}/\lambda_{em}$ = 288/345 nm owing to the energy transfer from the N/S-doped CQDs. The proposed method was found to be simple, reliable, and applicable for the determination of β-hCG with a wide range of analysis and high accuracy and precision.

Conflicts of interest

The authors declare no conflict of interest.

Acknowledgements

Authors extend their appreciation to the Deputyship for Research & Innovation, Ministry of Education in Saudi Arabia for funding this research work through the project number "NBU-FFR-2023-0020"

References

1 Y. Wang and A. Hu, Carbon quantum dots: synthesis, properties and applications, *J. Mater. Chem. C*, 2014, **2**, 6921–6939.
2 A. Sharma and J. Das, Small molecules derived carbon dots: synthesis and applications in sensing, catalysis, imaging, and biomedicine, *J. Nanobiotechnol.*, 2019, **17**, 92.
3 M. Nasrollahzadeh, M. Sajjadi, S. Mohammad Sajadi and Z. Issaabadi, *Chapter 5 – Green Nanotechnology, Interface Science and Technology*, Elsevier, 2019, vol. 28, pp. 145–198.
4 J. Liu, R. Li and B. Yang, Carbon Dots: A New Type of Carbon-Based Nanomaterial with Wide Applications, *ACS Cent. Sci.*, 2020, **6**, 2179–2195.
5 J. V. Klavins, Advances in biological markers for cancer, *Ann. Clin. Lab. Sci.*, 1983, **13**, 275.
6 M. T. Sheaff, J. E. Martin, D. F. Badenoch and S. I. Baithun, ß-hCG as a prognostic marker in adenocarcinoma of the prostate, *J. Clin. Pathol.*, 1996, **49**, 329–332.
7 U. Otite, S. Baithun, F. Chinegwundoh, V. H. Nargund and R. K. Iles, Detection of Human Chorionic Gonadotrophin in Serum or Urine of Prostate Cancer Patients Is of No Clinical Significance, *Tumor Biol.*, 2006, **27**(4), 181–186.
8 S. K. Sengodan, R. Nadhan, R. S. Nair, S. K. Hemalatha, V. Somasundaram, R. R. Sushama, A. Rajan, N. R. Latha, G. R. Varghese, R. Thankappan, J. M. Kumar, A. Chil, T. V. Anilkumar and P. Srinivas, BRCA1 regulation on β-hCG: a mechanism for tumorigenicity in BRCA1 defective breast cancer, *Oncogenesis*, 2017, **6**, e376.
9 S. P. Georgia Chris, L. P. Ravandhu and B. K. Haseena, *International Conference on Signal Processing Image Processing & Pattern Recognition (ICSIPR)*, 2013, vol. 75.
10 M. Daja, M. Aghmesheh, K. Ow, P. Rohde, K. D. Barrow and P. Russell, Beta-human chrionic gonadrtropin in semen: a marker for early detection of prostate cancer?, *Mol. Urol.*, 2000, **4**(4), 421–427.
11 P. N. Span, C. M. G. Thomas, J. J. Heuvel, R. R. Bosch, J. A. Schalken, L. vd Locht, E. J. B. M. Mensink and C. G. J. Sweep, Analysis of expression of chorionic gonadotrophin transcripts in prostate cancer by quantitative Taqman and a modified molecular beacon RT-PCR, *J. Endocrinol.*, 2002, **172**(3), 489–495.
12 J. Malakova, P. Pavek, I. Svecova, P. Zivny and V. Palicka, *J. Chromatogr. B*, 2009, **877**, 3226.
13 O. Stern and M. Volmer, Über die abklingzeit der fluoreszenz, *Z. Med. Phys.*, 1919, **20**, 183–188.
14 R.-Y. Xu, X.-F. Zhu, Y. Yang and P. Ye, High-sensitive cardiac troponin T, *J. Geriatr. Cardiol.*, 2013, **10**, 102–109.
15 E. M. Antman, Decision making with cardiac troponin tests, *N. Engl. J. Med.*, 2002, **346**, 2079–2082.
16 S. H. Jin, D. H. Kim, G. H. Jun, S. H. Hong and S. Jeon, Tuning the photoluminescence of graphene quantum dots through the charge transfer effect of functional groups, *ACS Nano.*, 2013, **7**, 1239–1245.
17 G. C. Semeraro, C. M. Cipolla and D. M. Cardinale, Role of Cardiac Biomarkers in Cancer Patients, *Cancers*, 2021, **13**, 5426.
18 Y. Liu, F. He, F. Gao, Y. Su, H. Wei and Y. Zhang, Nitrogen-doped, carbon-rich, highly photoluminescent carbon dots from ammonium citrate, *Nanoscale*, 2014, **6**, 1890–1895.
19 K. Thygesen, J. Mair, H. Katus, *et al.*, Recommendations for the use of cardiac troponin measurement in acute cardiac care, *Eur. Heart J.*, 2010, **31**, 2197–2204.
20 A. H. Wu, R. Valdes Jr, F. S. Apple, *et al.*, Cardiac troponin-T immunoassay for diagnosis of acute myocardial infarction, *Clin. Chem.*, 1994, **40**, 900–907.
21 M. Muller-Bardorff, K. Hallermayer, A. Schroder, *et al.*, Improved troponin T ELISA specific for cardiac troponin T isoform: assay development and analytical and clinical validation, *Clin. Chem.*, 1997, **43**, 458–466.
22 K. Hallermayer, D. Klenner and R. Vogel, Use of recombinant human cardiac Troponin T for standardization of third generation Troponin T methods, *Scand. J. Clin. Lab. Invest., Suppl.*, 1999, **230**, 128–131.
23 E. Giannitsis, K. Kurz, K. Hallermayer, *et al.*, Analytical validation of a high-sensitivity cardiac troponin T assay, *Clin. Chem.*, 2010, **56**, 254–261.
24 X. Wang, L. Cao, S. T. Yang, F. Lu, M. J. Meziani, L. Tian, K. W. Sun, M. A. Bloodgood and Y. P. Sun, Bandgap-like strong fluorescence in functionalized carbon nanoparticles, *Angew. Chem., Int. Ed.*, 2010, **49**, 5310–5314.
25 G. Eda, Y. Y. Lin, C. Mattevi, H. Yamaguchi, H. A. Chen, I. S. Chen, C. W. Chen and M. Chhowalla, Blue photoluminescence from chemically derived graphene oxide, *Adv. Mater.*, 2010, **22**, 505–509.
26 D. Sun, R. Ban, P.-H. Zhang, G.-H. Wu, J.-R. Zhang and J.-J. Zhu, Hair fiber as a precursor for synthesizing of sulfur-and nitrogen-codoped carbon dots with tunable luminescence properties, *Carbon*, 2013, **64**, 424–434.
27 M. Jorns and D. Pappas, A review of fluorescent carbon dots, their synthesis, physical and chemical characteristics, and applications, *Nanomaterials*, 2021, **11**(No), 1448.

28 J. Xu, Q. Liang, Z. Li, V. Y. Osipov, Y. Lin, B. Ge, Q. Xu, J. Zhu and H. Bi, Rational Synthesis of Solid-State Ultraviolet B Emitting Carbon Dots via Acetic Acid-Promoted Fractions of sp3 Bonding Strategy, *Adv. Mater.*, 2022, **34**, 2200011.

29 S. Yang, L. Zhi, K. Tang, X. Feng, J. Maier and K. Müllen, Efficient synthesis of heteroatom (N or S)-doped graphene based on ultrathin graphene oxide-porous silica sheets for oxygen reduction reactions, *Adv. Funct. Mater.*, 2012, **22**, 3634–3640.

30 Z. Yang, Z. Yao, G. Li, G. Fang, H. Nie, Z. Liu, X. Zhou, X. Chen and S. Huang, Sulfur-Doped Graphene as an Efficient Metal free Cathode Catalyst for Oxygen Reduction, *ACS Nano*, 2012, **6**, 205–211.

31 Y. Li, Y. Hu, Y. Zhao, G. Shi, L. Deng, Y. Hou and L. Qu, An electrochemical avenue to green-luminescent graphene quantum dots as potential electron-acceptors for photovoltaics, *Adv. Mater.*, 2011, **23**, 776–780.

32 J. Zhou, Y. Yang and C.-y. Zhang, A low-temperature solid-phase method to synthesize highly fluorescent carbon nitride dots with tunable emission, *Chem. Commun.*, 2013, **49**, 8605–8607.

33 Y. Dong, H. Pang, H. B. Yang, C. Guo, J. Shao, Y. Chi, C. M. Li and T. Yu, Carbon-based dots co-doped with nitrogen and sulfur for high quantum yield and excitation-independent emission, *Angew. Chem., Int. Ed.*, 2013, **52**, 7800–7804.

34 W. Horrocks and D. R. Sudnick, *J. Am. Chem. Soc.*, 1979, **101**, 334.

35 J. C. G. Bünzli and G. R. Choppin, *Lanthanide probes in life, chemical and earth sciences: theory and practise*, Elsevier, Amsterdam, 1989.

36 ICH, *Validation of Analytical Procedures: Text and Methodology, Q2(R1), Complementary Guideline on Methodology*, ICH, London, 2005.

37 M. S. Attia, M. H. Khalil, M. S. A. Abdel-Mottaleb, M. B. Lukyanova, Yu. A. Alekseenko and B. Lukyanov, Effect of Complexation with Lanthanide Metal Ions on the Photochromism of (1,3,3-Trimethyl-5-Hydroxy-6-FormylIndoline-Spiro2,2-[2H] chromene) in Different Media, *Int. J. Photoenergy*, 2006, 1–9.

38 M. S. Attia, M. H. Khalil, M. S. A. Abdel-Mottaleb, M. B. Lukyanova, Y. A. Alekseenko and B. Lukyanov, *Int. J. Photoenergy*, 2006, 1–9.

39 M. S. Attia, A. O. Youssef and A. A. Essawy, *Anal. Methods*, 2012, **4**, 2323–2328.

40 M. S. Attia, W. H. Mahmoud, A. O. Youssef and M. S. Mostafa, *J. Fluoresc.*, 2011, **21**, 2229–2235.

41 M. S. Attia, M. N. Ramsis, L. H. Khalil and S. G. Hashem, *J. Fluoresc.*, 2012, **22**, 779–788.

42 M. S. Attia, W. H. Mahmoud, M. N. Ramsis, L. H. Khalil, A. M. Othman, S. G. Hashem and M. S. Mostafa, *J. Fluoresc.*, 2011, **21**, 1739–1748.

43 M. S. Attia, A. M. Othman, E. Elraghi and H. Y. Aboul-Enein, *J. Fluoresc.*, 2011, **21**, 739–745.

44 A. A. Elabd and M. S. Attia, *J. Lumin.*, 2016, **169**, 313–318.

45 M. S. Attia, E. Bakir, A. A. Abdel-Aziz and M. S. A. Abdel-Mottaleb, *Talanta*, 2011, **84**, 27–33.

46 *FDA Guidance for Industry – Analytical Procedures and Method Validation, Chemistry, Manufacturing, and Controls Documentation*, Center for Drug Evaluation and Re- search (CDER) and Center for Biologics Evaluation and Research (CBER), 2000.

47 USP 31, *General Tests, Chapter 621 – Chromatography System Suitability, United States Pharmacopeial Convention (USP)*, Rockville, MD, 2009.

48 C. C. Chan, *et al.*, *Analytical Method Validation and Instrument Performance Verifıcation*, John Wiley & Sons (Wiley Interscience), Hoboken, NJ, 2004.

49 M. S. Attia, S. A. Elsaadany, K. A. Ahmed, M. M. El-Molla and M. S. A. Abdel-Mottaleb, *J. Fluoresc.*, 2015, **25**, 119–125.

50 S. G. Hashem, M. M. Elsaady, H. G. Afify, M. El-Kemary and M. S. Attia, *Talanta*, 2019, **199**, 89–96.

51 M. S. A. Abdel-Mottaleb, M. Saif, M. S. Attia, M. M. Abo-Aly and S. N. Mobarez, *Photochem. Photobiol. Sci.*, 2018, **17**, 221–230.

52 W. E. Omer, M. A. El-Kemary, M. M. Elsaady, A. A. Gouda and M. S. Attia, *ACS Omega*, 2020, **5**, 5629–5637.

53 L. M. Abdullah, M. S. Attia and M. S. A. Abdel-Mottaleb, *Egypt. J. Chem.*, 2019, **62**, 247–255.

54 M. S. Attia, A. O. Youssef, A.-S. S. H. Elgazwy, S. M. Agami and S. I. Elewa, *J. Fluoresc.*, 2014, **24**, 759–765.

55 M. M. Abd-Elzaher, M. A. Ahmed, A. B. Farag, M. S. Attia, A. O. Youssef and S. M. Sheta, *Sens. Lett.*, 2017, **15**(12), 977–981.

56 V. Bressi, A. Ferlazzo, D. Iannazzo and C. Espro, *Nanomaterials*, 2021, **11**(5), 1120.

57 M. Díaz-Álvarez and A. Martín-Esteban, *Biosensors*, 2021, **11**(3), 79.

58 K. Murugan, V. Kumar Jothi, A. Rajaram and A. Natarajan, *ACS Omega*, 2022, **7**(1), 1368–1379.